PAPER

Novel polyethersulfone (PES)/hydrous manganese dioxide (HMO) mixed matrix membranes with improved anti-fouling properties for oily wastewater treatment process

R. Jamshidi Gohari,[ab] E. Halakoo,[a] W. J. Lau,[a] M. A. Kassim,[a] T. Matsuura[ac] and A. F. Ismail*[a]

In this work, hydrophilic hydrous manganese dioxide (HMO) nanoparticles were synthesized and used as the inorganic filler for the preparation of mixed matrix membranes (MMMs). The aim of adding HMO nanoparticles into the polyethersulfone (PES) membrane matrix is to improve membrane hydrophilicity and anti-fouling resistance against oil deposition and/or adsorption. The resulting membranes were characterized by SEM, AFM, FTIR, contact angle measurements and ultrafiltration (UF) of synthetic oily wastewater. Experimental results showed that the hydrophilicity of the PES/HMO membrane was significantly improved to a low value of contact angle (16.4°) by HMO loading, which as a consequence led to a promising pure water permeability (573.2 L m^{-2} h^{-1} bar^{-1}). In comparison, the pristine PES membrane only demonstrated 69.5° and 39 L m^{-2} h^{-1} bar^{-1}, respectively. Furthermore, the PES/HMO membrane exhibited an excellent oil rejection (almost 100%) and a promising water flux recovery (75.4%) when it was used to treat a synthetic oily solution containing 1000 ppm oil. The promising anti-fouling properties of the PES/HMO membrane could be attributed to the presence of hydrophilic −OH groups on the membrane surface resulting from HMO addition, making this membrane less susceptible to fouling when challenged with oil-in-water emulsions.

1. Introduction

Industrially, oil and gas operations are among the sectors that produce the largest amounts of wastewater which contains not only a high amount of oil and grease but also other minor toxic components.[1] Because of this, the wastewater must be properly treated before discharging into any receiving water body in order to protect aquatic life. The presence of oil and grease in wastewater can be seen in different forms such as free, dispersed or emulsified which predominantly have differences in size.[2,3] In most of the cases, the oil droplets are spread extremely well in small droplet of less than 10 μm, making the conventional techniques such as gravity separation, centrifugation and air flotation ineffective in separating them from the wastewater.[2,4–8] Typical oily wastewaters may contain between 50 and 1000 ppm total oil and grease (TOG), depending on the

[a]Advanced Membrane Technology Research Centre (AMTEC), Universiti Teknologi Malaysia, 81310 Skudai, Johor, Malaysia. E-mail: afauzi@utm.my; Fax: +60 7 558 1463; Tel: +60 7 553 5592

[b]Department of Chemical Engineering, Islamic Azad University, Bardsir Branch, Bardsir, Iran

[c]Industrial Membrane Research Laboratory, Department of Chemical and Biological Engineering, University of Ottawa, 161 Louis Pasteur St, Ottawa, ON K1N 6N5, Canada

type of application. The maximum content of TOG in discharge water however is limited to 5–40 ppm according to regulations, with a typical requirement of 10–15 ppm.[1,2] In view of this, the use of ultrafiltration (UF) membrane as treatment technology has offered a potential alternative solution to tackle the problem owing to its unique advantages such as excellent separation efficiency, easy operation, low energy and maintenance costs and no chemical use.[9–11] As UF membranes have sub-micron pore size on their surface, they are in general very effective in separating small oil droplets even at operating pressure of less than 1 bar.[2,5,6,12–14]

Chakrabarty et al.[2,15] in their two different published works have investigated the performance of several kinds of polysulfone (PSF) membranes made of different additives in the treatment of oily wastewater and found that almost all of the membranes tested were able to reject more than 90% of oil molecules when tested with feed solution of 100 mg L^{-1} oil. Lee and Frankiewicz[16] on the other hand used a hydrophilic UF membrane in a cross-flow mode to treat oily wastewater. By incorporating this UF membrane with hydrocyclone as pretreatment process, a permeate of high quality was able to produce (with TOC less than 2 mg L^{-1}) even though the feed oil concentration was varied between 100 and 1000 ppm. Wu et al.[17] also reported that a hydrophilic polyvinyl alcohol (PVA) UF

membrane could reject more than 96.5% oil with permeate flux recorded at 360 L m^{-2} h^{-1} when tested with 806.75 mg L^{-1} oil solution at operating pressure of 2 bar. Although previous studies have showed that UF membrane has encountered no major problem in treating oily wastewater, its susceptibility to fouling problem still remains a main concern to many. The membrane fouling problems resulted from oil adsorption and deposition has negative impacts on water permeability, causing it to deteriorate as a function of time if proper cleaning process is not frequently conducted.[2,5,7,11,18–22] Although optimizing filtration conditions could reduce membrane fouling tendency to certain extent, many researchers believed that improving membrane hydrophilicity itself is the most sustainable solution in minimizing fouling propensity.[6,9,12,23,24]

Several studies have reported the use of membranes made of either PSF or polyethersulfone (PES) or polyvinylidene difluoride (PVDF) polymer for oily wastewater treatment process, but the hydrophobic nature of these polymers is the main concern that is strongly linked to fouling in long run.[19,25,26] In order to improve the hydrophilicity of these membranes, attempts have been made to incorporate the membrane with different types of hydrophilic inorganic fillers with the aims of not only improving membrane hydrophilicity but also its water permeability and anti-fouling resistance.[6,9,25,27] This kind of membrane comprising both organic and inorganic material is denoted as a 'mixed matrix membrane' (MMM) and is able to demonstrate the positive features of each material, achieving the synergistic effect for membrane performance enhancement.

Zhang et al.[9] reported that inorganic metal oxide particles are able to increase the membrane capability and performance during oily wastewater treatment process. Their findings showed that both hydrophilicity and anti-fouling property of membrane could be enhanced upon addition of sulfated Y-doped nonstoichiometric zirconia to PSF membrane matrix. The addition of inorganic nano-sized alumina particles (Al$_2$O$_3$) to PVDF membrane was also evaluated by Li et al.[6] They experienced that the modified PVDF membrane was able to enhance water flux of unmodified membrane by two orders without compromising its good separation efficiency. The improved membrane performance might be attributed to the hydrophilic effect of Al$_2$O$_3$ which could improve not only membrane permeability but also its antifouling performance. In the study by Yuliwati et al.,[10] they embedded hydrophilic titanium dioxide (TiO$_2$) nanoparticles in PVDF membrane and used the membrane to treat oily wastewater under submerged conditions. As reported, the membrane surface was altered and was able to demonstrate balance performance of permeability and selectivity when the membrane was subject to a synthetic oily wastewater. Ahmad et al.[28] also carried out research work on modification of PSF UF membrane using inorganic silica (SiO$_2$) nanoparticles. The improved properties of the PSF–SiO$_2$ membrane with respect to hydrophilicity and antifouling resistance have been evidenced during filtration process of oil-in-water emulsion.

Considering the advantages of inorganic particles for membrane performance enhancement, the aim of this study was to synthesize highly hydrophilic MMMs with improved performance and fouling resistance by incorporating PES membrane with self-synthesized nanoparticles, i.e. hydrous manganese dioxide (HMO). The performances of the resulting MMMs were characterized with respect to water permeability, oil rejection and water flux recovery in addition to the instrumental characterizations using contact angle goniometer, FTIR, SEM and AFM.

2. Experimental

2.1 Materials

PES (Radel® A300, MW: ~15 000 g mol^{-1}) was purchased from Amoco Chemicals. Manganese(II) sulfate monohydrate (MnSO$_4$·H$_2$O), potassium permanganate (KMnO$_4$) and sodium hydroxide (NaOH) supplied by Merck were used to synthesize inorganic hydrophilic HMO nanoparticles. Polyvinylpyrrolidone (PVP) (MW: 24 000 g mol^{-1}) and N-methyl-2-pyrrolidinone (NMP) obtained from Merck were used as pore forming agent and solvent, respectively. DI water was used in all procedures.

2.2 Preparation of HMO nanoparticles

Inorganic HMO nanoparticles were synthesized via oxidation of manganous ions by permanganate in accordance to the Parida's method.[29] A solution was first prepared by dissolving 40 g of KMnO$_4$ in 500 mL DI water (with pH of the solution adjusted to 12.5 using 1 M NaOH solution). Then, the resulting solution was added dropwise to an equal volume of aqueous solution containing 60 g of MnSO$_4$·H$_2$O under vigorous stirring until the brownish precipitates appeared. Afterwards, the resulting product, HMO powder, was filtered and washed several times with DI water. Finally, the synthesized HMO nanoparticles were heated in vacuum oven at 60 °C for 24 h, followed by grinding before storing in a desiccator until use.

2.3 UF membrane preparation

In this study, the PES and PES/HMO UF MMMs were fabricated by immersion precipitation (i.e. phase inversion) method, and the process was as follows:

(1) *Preparation of dope solution*: A predetermined amount of PVP was first dissolved in NMP solvent. HMO inorganic particles were then added into the solution and dispersed sufficiently well with stirring, followed by sonication at 50 °C for several hours. Dried PES polymer pellets were then added into the mixture and stirred at 500 rpm for 24 h until a homogenous suspension was obtained. The dope solution for the pristine PES membrane was prepared in the same way without adding HMO particles. The viscosity of dope solutions were measured by a basic viscometer (Model: 98965-40, Cole-Parmer).

(2) *Preparation of flat sheet MMM*: The uniform suspension above prepared was poured onto a smooth glass plate and cast by a casting blade at a speed of 5 cm s^{-1} to form a film of 250 μm thickness. The cast film together with the glass plate was then immersed into a DI water bath for a few minutes for phase inversion to take place. Once the membrane was peeled off naturally from the glass plate, it was transferred to another water bath where it was kept for another 3 days to completely

remove residual solvent and PVP. The membrane was then dried at room temperature (with humidity between 60 and 70%) prior to use. Table 1 shows the composition of the dope solution used for fabricating different types of membranes.

2.4 Filtration experiments

2.4.1 Preparation of oily wastewater.
The synthetic oily wastewater was prepared using crude oil obtained from Terengganu Crude Oil Terminal (Location: RE110) which is located offshore of the east of peninsular Malaysia. The crude oil-in-water emulsion was prepared by mixing crude oil of different concentrations, *i.e.* 100, 200, 500 and 1000 ppm, with DI water under vigorous stirring at 350 rpm for about 30 min at room temperature. Once the process was completed, a solution with uniform yellowish colour was obtained. Considering coalescence of oil droplets that may occur during a prolonged period of storage, synthetic wastewater was prepared a day before experiment to keep the feed characteristics consistent. The oil droplet size in the synthetic wastewater of 1000 ppm was determined by Zetasizer Nano ZS (Malvern Instrument Inc.) with refractive index of 1.5 and 1.333 for the oil droplets and dispersant (water), respectively and the results obtained at different pH environments are shown in Table 2.

2.4.2 Cross-flow UF experiment.
For the cross-flow UF experiments, the membranes were first evaluated with respect to pure water flux before subjecting to the synthetic oily solutions of various properties. Prior to the permeation tests, all the membranes with an effective area of around 12.56 cm^2 each were pressurized at 1 bar for a period of 30 min in order to achieve steady-state flux. Pure water flux of membrane (J_{w1}) which was evaluated at 1 bar could be calculated using eqn (1).[30]

$$J_{w1} = \frac{V}{A \times t} \qquad (1)$$

where V, A and t are the volume of permeated pure water (L), the effective area of the flat sheet membrane (m^2) and the operation time (h), respectively. This equation was also employed to calculate the permeate flux of membranes when they were used to treat synthetic oily solutions. For the water treatment experiments, two important variables, *i.e.* oil concentration and feed pH value were considered in which the oil concentration of the synthetic oily water was varied in the range of 100–1000 ppm while the pH was changed in the range of 3–9. The permeate was taken every 10 min (up to 2 h) in order to evaluate the effects of oil concentration and pH value on the permeate flux and oil rejection of membranes. To determine the rejection of membrane against crude oil at different feed conditions, the following equation was employed.[30]

Table 2 The average oil droplet size (diameter) and droplet size range in different pH environment

pH	Average (nm)	Droplet size range (nm)
3	277.7	60–7000
7	386.8	85–8200
9	467.2	100–8500

$$R(\%) = \left(1 - \frac{C_p}{C_f}\right) \times 100 \qquad (2)$$

where C_p and C_f are the concentration of oil in the permeate and the feed (mg L^{-1}), respectively. UV-vis spectrophotometer (Model: DR5000, Hach) was used to determine the oil concentration of samples at the wavelength of around 305 nm. In order to obtain the flux recovery ratio (R_{FR}) of membrane, the feed solution tank was refilled with DI water after 2 h of UF of synthetic oily solution and the membrane was rinsed by letting the DI water flow thoroughly for 30 min under the same condition as pure water permeation test. Then, the pure water flux (J_{w2}) was re-evaluated to obtain R_{FR} using eqn (3).[31]

$$R_{FR}(\%) = \left(\frac{J_{w2}}{J_{w1}}\right) \times 100 \qquad (3)$$

2.5 Membrane characterization

2.5.1 Overall porosity.
The membrane porosity (ε) was calculated by the following equation.[32]

$$\varepsilon(\%) = \left(\frac{W_w - W_d}{\rho \times A \times L}\right) \times 100 \qquad (4)$$

where W_w and W_d are the weight of wet and dry membrane (g), respectively; A, the effective area of the membrane (cm^2); ρ, the density of water; L the wet membrane thickness (cm). A circular membrane piece was weighed (W_d) after vacuum drying for 24 h at 50 °C. Then, the membrane was immersed in DI water overnight and weighed (W_w) after the surface was blotted with a filter paper.

2.5.2 Transmission electron microscopy.
Transmission electron microscope (TEM) (Model: HT 7700, Hitachi) was used to analyze the morphology and determine particle size of the synthesized HMO nanoparticles. Prior to the analysis, the fine HMO particles were dispersed in absolute alcohol and were sonicated for 10 min to produce homogenous suspension. A droplet of this suspension was then placed on a coated grid before drying in vacuum oven at 60 °C for 1 h.

2.5.3 Scanning electron microscopy.
Scanning electron microscope (SEM) (Model: TM 3000, Hitachi) equipped with

Table 1 Composition of the dope solution for membrane preparation

Membrane	HMO/PES ratio	PES (wt%)	PVP (wt%)	NMP (wt%)	HMO (wt%)	Viscosity (cp)
PES	0	15.00	1.50	83.50	—	203
PES/HMO-1	1	13.04	1.30	72.60	13.04	415
PES/HMO-2	2	11.54	1.15	64.23	23.08	1118

energy dispersive X-ray spectroscope (EDX) (Model: X-flash min SVE, Bruker) was used to monitor the morphology of the pristine PES membrane and the PES/HMO MMMs. Prior to scanning, the cross-sectional membrane samples were prepared by freeze-fracturing in liquid nitrogen to prevent the collapse of the porous structure. The membrane was later sputter-coated with gold to avoid charging during SEM analysis.

2.5.4 Fourier-transform infrared spectroscopy. ATR-FTIR spectroscope (Model: UATR, Perkin Elmer) was conducted to investigate the changes of functional groups and elements in the inorganic HMO nanoparticles and PES/HMO MMMs. The IR spectrum for the nanoparticles was obtained *via* the KBr pellet technique.

2.5.5 X-ray diffractometry. X-ray diffraction patterns of the synthesized HMO particles and all fabricated membranes were recorded by an X-ray diffractometer (Model: D5000, Siemens) equipped with monochromatic Cu Kα radiation at diffraction angle 2θ in the range of 10–90°.

2.5.6 Atomic force microscopy. Surface morphology of fabricated membranes was visualized by atomic force microscope (AFM) (Model: SPA-300 HV, Seiko). The scan was made over an area of 10 μm × 10 μm to obtain surface roughness and pore size by tapping mode at room temperature of 25 °C. The mean roughness, R_a, representing the mean value of the surface relative to the center plane for which the values enclosed by the images above and below this plane are equal was obtained from the line profiles at different locations chosen arbitrarily for each membrane sample using the AFM software program.[33] The surface pore size of the membranes was measured by visually inspecting the line profiles of various pores observed on AFM image at different areas of the same membrane.[34]

2.5.7 Contact angle measurement. To determine membrane surface hydrophilicity, the water contact angle of the membranes was measured by sessile drop method using an automated contact angle goniometer (Model: OCA 15plus, DataPhysics). A droplet of DI water with a volume of 0.5 μL was carefully formed at ten spots randomly chosen on the membrane surface using a motor-driven microsyringe and the average value was reported.

3. Results and discussion

3.1 Morphology of HMO nanoparticles

The morphology and particle size of the synthesized HMO nanoparticles is shown in Fig. 1 at different scale bar. As can be clearly seen, the synthesized HMO nanoparticles are a mixture of flake-like shape particles with the average particle size of smaller than 6 nm and needle-shaped particles with the average size of 12 nm in diameter.

3.2 Functional groups of membranes

The ATR-IR spectra of inorganic HMO nanoparticles, pristine PES membrane and PES/HMO-2 membrane are shown in Fig. 2. The HMO nanoparticles spectrum depicts the O–H stretching vibration band at around 3292 cm^{-1} and the O–H bending vibration combined with Mn atom at band of 1625 cm^{-1}.[35] The weak bands in the wavenumber region between 400 and 900 cm^{-1} are due to
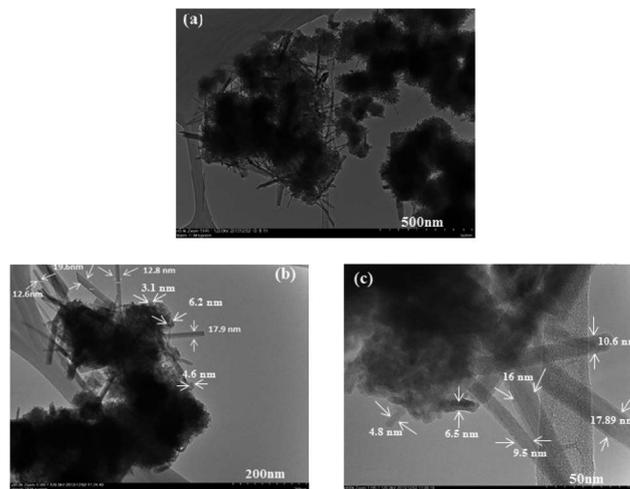

Fig. 1 Morphology and particle size of synthesized HMO particles captured at different scale bars, (a) 500 nm, (b) 200 nm and (c) 50 nm.
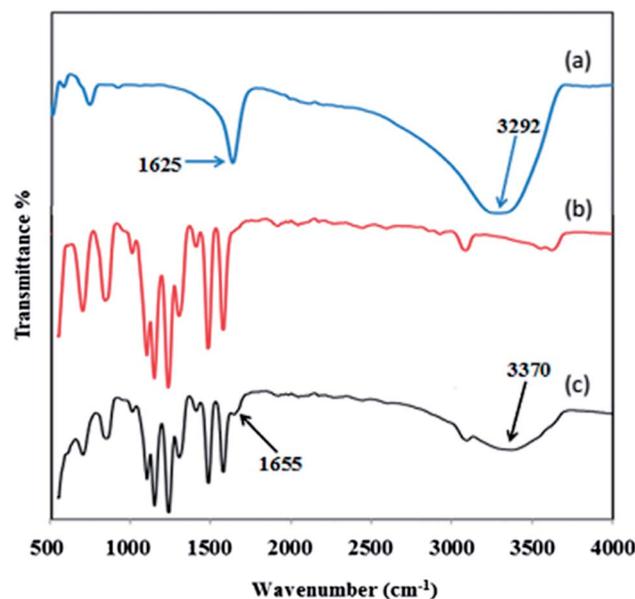

Fig. 2 FTIR spectra of (a) HMO nanoparticles, (b) pristine PES membrane and (c) PES/HMO-2 membrane.

the presence of MnO$_6$ octahedra in the synthesized nanoparticles.[35,36] Compared to the PES membrane, the presence of two new characteristic peaks at 1655 and 3370 cm^{-1} in PES/HMO-2 membrane confirms the successful incorporation of HMO particles in the membrane matrix. Since there is no evidence (new peak) showing the chemical bonding between HMO nanoparticles and PES membrane in the present work, it is reasonable to say that the interaction of organic membrane and inorganic filler is mainly based on physical interaction.

3.3 XRD of membranes

Fig. 3 depicts the XRD patterns of HMO nanoparticles and PES membrane embedded with and without HMO nanoparticles.

Two strong peaks are obvious at 2θ of 45.2° and 76° in the HMO nanoparticles and these can be ascribed to the typical characteristic peaks of amorphous HMO nanoparticles. Compared to the pristine PES membrane, two significant peaks observed at 2θ of 45.2° and 76° in PES/HMO-2 MMM is the strong indication confirming the presence of HMO nanoparticles in the PES membrane matrix.

3.4 Membrane hydrophilicity

Surface hydrophilicity of membrane plays an important role to define the pure water flux and antifouling property. Fig. 4 presents the contact angle values of the PES membranes with different loadings of HMO nanoparticles. The contact angle value and subsequently pure water flux changed from 69.5° and 39.2 L m^{-2} h^{-1} of pristine PES membrane to 42.3° and 336 L m^{-2} h^{-1} of PES/HMO-1 membrane and to 16.4° and 573.2 L m^{-2} h^{-1} of PES/HMO-2 membrane with increasing HMO : PES ratio from zero to 2. Thus, the effect of HMO loading on the hydrophilicity of the membranes is obvious. This is due to the superhydrophilic nature of HMO with many –OH functional groups.[25,37–39] It should be taken into account that the hydroxyl groups of nanoparticles are able to interact with water molecules easily through the hydrogen bonding and the van der Waals force, which leads to an increase in water permeability as evidenced in previous studies.[26,40]

3.5 Morphological analysis using SEM

The SEM micrographs of the surface and the cross-section of the pristine PES membrane and the MMMs are shown in Fig. 5. The formation of asymmetric structure, which consists of a porous skin layer supported by a finger-like sublayer, is the typical result of the phase inversion process adopted in this work for membrane fabrication. It is obvious that by increasing the weight ratio of HMO : PES the finger-like pores become
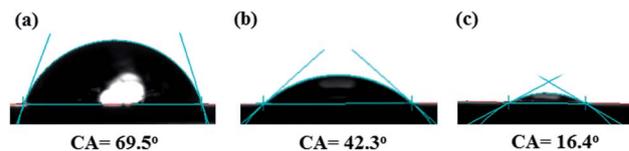

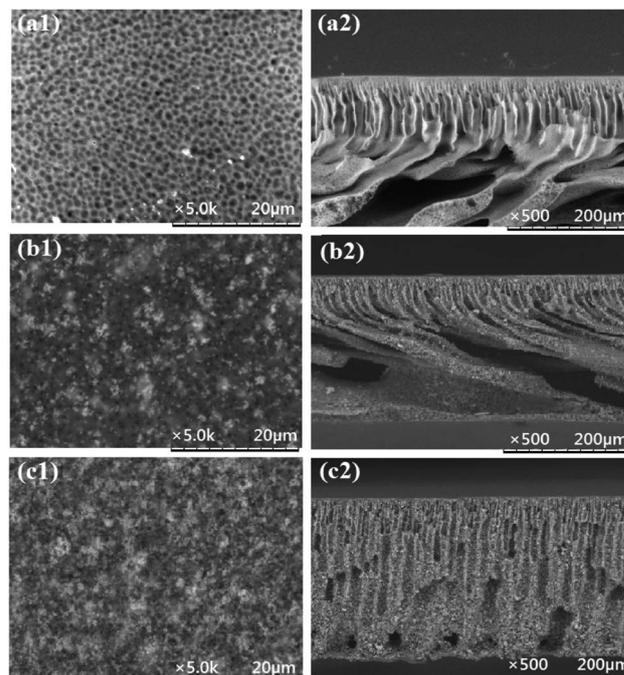**Fig. 4** Water contact angle of membranes, (a) PES, (b) PES/HMO-1 and (c) PES/HMO-2 membrane.

Fig. 5 SEM images of top surface (magnification of 5000×) and cross section (magnification of 500×) of PES membranes prepared from different nanoparticles loadings, (a) PES, (b) PES/HMO-1 and (c) PES/HMO-2 membrane.
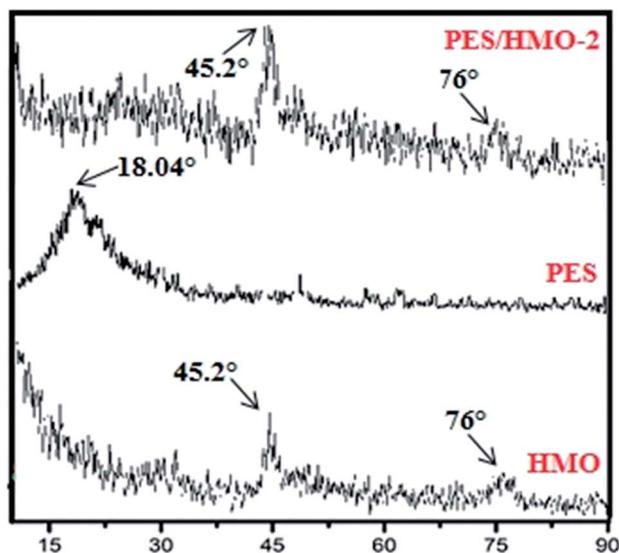

Fig. 3 Comparison between the XRD patterns of HMO particles and PES membrane embedded with and without HMO particles.

longer and finally, they become the vertically oriented macrovoids of PES/HMO-2. It is observed from the top layer images that with increase in the HMO loading the pore size tends to decrease. It can be easily observed that HMO particles are uniformly dispersed along the entire cross-section, which indicates that sedimentation nanoparticles does not occur during MMM preparation.[9] Increase of surface hydrophilicity with HMO loading is obviously due to abundance of hydrophilic –OH groups at the MMM surface. The improved membrane hydrophilicity upon addition of HMO nanoparticles is consistent with FTIR observation and contact angle results. Table 3 shows the results of EDX analysis on the top surface of membranes with respect to carbon (C), oxygen (O), sulfur (S) and manganese (Mn) atomic elements. The results further confirm the successful incorporation of HMO nanoparticles in the membrane matrix and the higher the HMO nanoparticles added, the higher the percent of Mn and O detected on membrane surface.

Table 3 EDX analysis of the top surface of membranes

Element	Membrane		
	PES (at.%)	PES/HMO-1 (at.%)	PES/HMO-2 (at.%)
C	74.71	59.33	50.19
O	18.99	28.04	33.58
S	6.30	3.62	2.39
Mn	—	9.01	13.84
Total	100.00	100.00	100.00

Table 4 Properties of membrane with respect to overall porosity, surface pore size and average roughness (R_a)

Membrane	Overall porosity (%)	Pore size (nm)	R_a (nm)
PES	80.5	146.6	2.96
PES/HMO-1	83.1	96.7	16.03
PES/HMO-2	87.9	76.4	35.51

3.6 Morphological analysis by AFM

Top-view AFM images of the pristine PES membrane and the MMMs over an area of 10 μm × 10 μm are shown in Fig. 6. As can be clearly seen from these images, the top surface morphology has been altered with the addition of HMO nanoparticles into the dope solution. The surface roughness increases and the edge and the valley of the rough surface become more oriented to the direction of the casting bar movement with an increase in HMO loading. The numerical values of the surface roughness are shown in Table 3. It increases from 2.96 nm of the pristine PES membrane to 16.03 and 35.51 nm of PES/HMO-1 and PES/HMO-2 membrane, respectively. Table 4 also presents the surface pore size of the membranes. The decrease in surface pore size and the increase in porosity with an increase in HMO loading is consistent with the SEM observation.

3.7 UF experiments for oily wastewater treatment process

3.7.1 Permeate flux and oil rejection. Fig. 7 shows the variation of permeation flux and oil rejection of the fabricated membranes as a function of operation time for the cross-flow UF experiment of wastewater containing 1000 ppm oil. Clearly, the permeate flux of membrane was in the order of PES/HMO-2 > PES/HMO-1 > PES membrane. Although this order coincides with the order of the pure water flux shown earlier, the permeate flux of oily wastewater is much lower than the pure water flux. This is due to the coverage of membrane surface by the oil layer. The flux tends to decrease from the initial value with time but even after leveling off PES/HMO-2 membrane maintained significantly higher flux (573.2 L m^{-2} h^{-1}) than the pristine PES membrane (39.4 L m^{-2} h^{-1}). The excellent permeate flux of PES/HMO-2 membrane is mainly attributed to improved membrane morphology (higher porosity) and the increased hydrophilicity.

With respect to oil rejection, it is observed that both PES/HMO membranes demonstrated significantly higher rejection than the pristine PES membrane throughout the entire experimental period. Almost complete oil rejection was able to be achieved by PES/HMO-2 membrane in comparison to 98.5–99.99% and 92.3–97.5% shown by PES/HMO-1 and PES membrane, respectively. There are two main factors contributing to the excellent performance of PES/HMO-2 membrane. The first one is due to the smallest surface pore size of the membrane which plays a main role in preventing oil particles from passing through the membrane. Although the average pore sizes of all the prepared membranes are smaller than the oil droplet size, a wide range of pore size distribution of the PES membrane may have allowed the passage of some oil droplets, thus lowering the oil rejection considerably. However, the pores are gradually blocked by the adsorption of oil at the membrane wall, which narrows the permeate flow channel. Thus, oil rejection of the PES membrane gradually increases with time. The second factor to be considered is the highest hydrophilicity of the PES/HMO-2 membrane, which minimized oil deposition and/or adsorption.

3.7.2 Flux recovery ratio. Fig. 8 shows the flux recovery ratio, defined by eqn (3), of the membranes. As the figure shows, there is substantial improvement of water flux recovery by HMO loading, *i.e.* 42%, 68% and ~75% for PES, PES/HMO-1 and PES/HMO-2 membrane, respectively. The high recovery ratio of the PES/HMO-2 also indicates its excellent antifouling property by reducing the formation of oil layer on membrane surface (and/or pore blocking by smaller oil droplet). As a conclusion, it can be said that hydrophilic HMO nanoparticle has a potential of enhancing membrane hydrophilicity and further its antifouling resistance against oil droplets during treatment of oily wastewater process.

3.7.3 Effect of oil concentration and pH. The influence of oil concentration on the permeate flux of PES/HMO-2
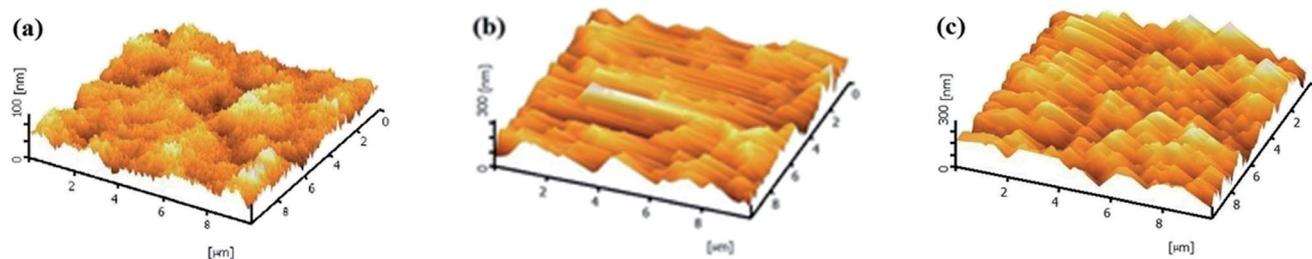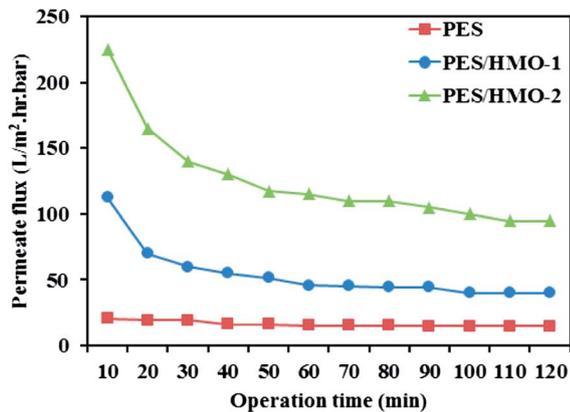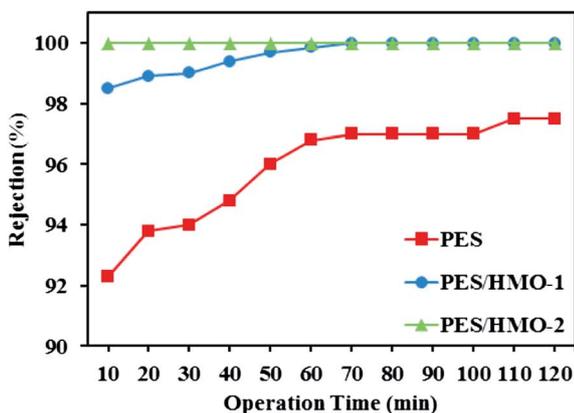

Fig. 6 3D surface AFM images of the membranes with different HMO/PES ratios, (a) PES, (b) PES/HMO-1 and (c) PES/HMO-2.

(a)

(b)

Fig. 7 Separation performance of PES and PES/HMO membranes in the treatment of synthetic oily wastewater (feed oil concentration: 1000 ppm and pH: 7) as a function of operation time, (a) permeate flux and (b) oil rejection.
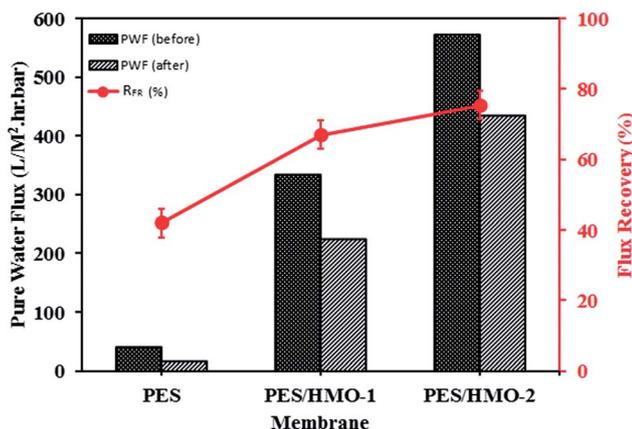

Fig. 8 Pure water flux of membrane before and after oily wastewater treatment and its flux recovery rate.

membrane was also investigated and the results are presented in Fig. 9. It is found that oil concentration has strong impact on permeate flux, *i.e.* the higher the oil concentration the greater

the flux decline. With respect to oil rejection, the membrane displayed almost complete rejection of oil regardless of the feed oil concentration. For every oil concentration, the flux leveled off within 90 min of operation. The flux decrease during the first hour of operation is attributed to the increase in resistance to permeation flow because of the formation of oil layer on the membrane surface. As can be seen from Fig. 10, increasing oil concentration in the feed solution had negative impact on water flux recovery. These results are due to the fact that the thicker oil layer is formed at the membrane surface while contacting with the feed containing the larger amount of oil droplets and simple water cleaning could not remove the adsorbed layer effectively.

The performance of the PES/HMO-2 membrane was further assessed by varying the pH of the synthetic oily solution of 1000 ppm oil using diluted HCl or NaOH solution to adjust the special values of pH and the results are shown in Fig. 11 as a function of operation time. Obviously, the permeate flux was affected by the feed pH and the permeate flux was increased by increasing the feed pH from 3 to 9. The lowest water
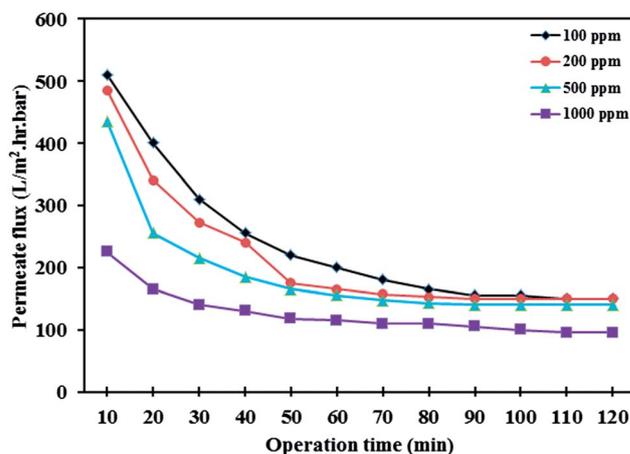

Fig. 9 Effect of oil concentration on the permeate flux of PES/HMO-2 membrane as a function of time.
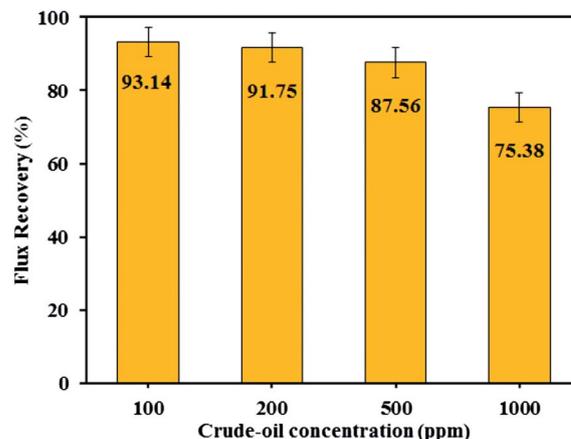

Fig. 10 Flux recovery rate of PES/HMO-2 membrane at different oil concentrations in the feed.
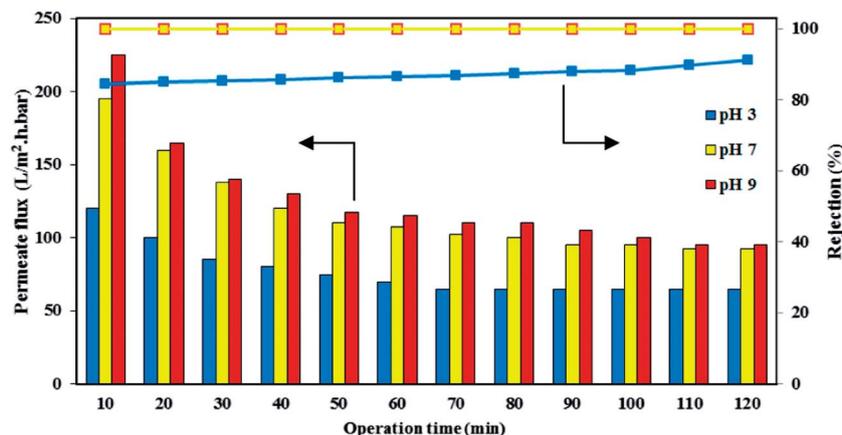
Fig. 11 Effect of feed pH on the permeate flux of PES/HMO-2 membrane.

permeability at the acidic environment obtained in this study is consistent with the findings of Hua *et al.*[41] in which they reported the water flux of MF membrane at pH 4 was much lower than at pHs 6 and 10 when the membrane was used to treat feed solution containing 500 ppm oil. However, Zhao *et al.*[42] reported a contradictory result that the flux of membrane decreased as the pH increased in the range of 2–10. Therefore, it can be said that the permeate flux under different pH values was not only affected by the membrane properties but also by the characteristic of oil droplets, particularly by the oil droplet size. Table 2 shows that the droplet sizes of oil were the smallest (average 277 nm with a range of 60–7000 nm) at pH 3. Thus, some of the droplets were accommodated by the membrane pore (average size of 76.4 nm), resulting in pore blockage and low permeate flux. As well, some of the smallest droplets permeated through the pores, lowering the oil rejection. As pH increases, oil size increases, which result in higher permeate flux and higher oil rejection.

4. Conclusions

In this work, an investigation was made on the separation of oil from the synthetic crude oil-in-water emulsion using PES/HMO MMMs. The results revealed that the addition of hydrophilic HMO nanoparticles into dope solution played a role in improving not only membrane hydrophilicity but also its water permeation rate and anti-fouling resistance against oil deposition and adsorption. Although the permeability of PES/HMO-2 membrane was significantly improved, its oil rejection rate was not compromised as the membrane was still able to produce permeate of high quality (almost complete rejection of oil) regardless of oil concentration and feed pH. In addition, at the highest HMO nanoparticles loading, the PES/HMO-2 membrane demonstrated the greatest flux recovery among the studied membrane, indicating its excellent anti-fouling properties in reducing oil deposition and/or adsorption. This study shows the potential of using HMO nanoparticles as alternative promising filler in improving PES membrane properties, making it suitable for treating oily wastewater.

References

1 J. Mueller, Y. Cen and R. H. Davis, Crossflow microfiltration of oily water, *J. Membr. Sci.*, 1997, **129**, 221–235.

2 B. Chakrabarty, A. K. Ghoshal and M. K. Purkait, Cross-flow ultrafiltration of stable oil-in-water emulsion using polysulfone membranes, *Chem. Eng. J.*, 2010, **165**, 447–456.

3 M. Cheryan and N. Rajagopalan, Membrane processing of oily streams. Wastewater treatment and waste reduction, *J. Membr. Sci.*, 1998, **151**, 13–28.

4 P. Srijaroonrat, E. Julien and Y. Aurelle, Unstable secondary oil/water emulsion treatment using ultrafiltration: fouling control by backflushing, *J. Membr. Sci.*, 1999, **159**, 11–20.

5 W. Chen, J. Peng, Y. Su, L. Zheng, L. Wang and Z. Jiang, Separation of oil/water emulsion using Pluronic F127 modified polyethersulfone ultrafiltration membranes, *Sep. Purif. Technol.*, 2009, **66**, 591–597.

6 Y. S. Li, L. Yan, C. B. Xiang and L. J. Hong, Treatment of oily wastewater by organic–inorganic composite tubular ultrafiltration (UF) membranes, *Desalination*, 2006, **196**, 76–83.

7 A. Lobo, Á. Cambiella, J. M. Benito, C. Pazos and J. Coca, Ultrafiltration of oil-in-water emulsions with ceramic membranes: Influence of pH and crossflow velocity, *J. Membr. Sci.*, 2006, **278**, 328–334.

8 N. Moulai-Mostefa, M. Frappart, O. Akoum, L. Ding and M. Y. Jaffrin, Separation of water from metal working emulsions by ultrafiltration using vibratory membranes, *J. Hazard. Mater.*, 2010, **177**, 978–982.

9 Y. Zhang, P. Cui, T. Du, L. Shan and Y. Wang, Development of a sulfated Y-doped nonstoichiometric zirconia/polysulfone composite membrane for treatment of wastewater containing oil, *Sep. Purif. Technol.*, 2009, **70**, 153–159.

10 E. Yuliwati and A. F. Ismail, Effect of additives concentration on the surface properties and performance of PVDF ultrafiltration membranes for refinery produced wastewater treatment, *Desalination*, 2011, **273**, 226–234.

11 X. S. Yi, W. X. Shi, S. L. Yu, C. Ma, N. Sun, S. Wang, L. M. Jin and L. P. Sun, Optimization of complex conditions by

response surface methodology for APAM–oil/water emulsion removal from aqua solutions using nano-sized TiO_2/Al_2O_3 PVDF ultrafiltration membrane, *J. Hazard. Mater.*, 2011, **193**, 37–44.

12 H.-J. Li, Y.-M. Cao, J.-J. Qin, X.-M. Jie, T.-H. Wang, J.-H. Liu and Q. Yuan, Development and characterization of anti-fouling cellulose hollow fiber UF membranes for oil–water separation, *J. Membr. Sci.*, 2006, **279**, 328–335.

13 C. S. Ong, W. J. Lau, P. S. Goh, B. C. Ng and A. F. Ismail, Preparation and characterization of PVDF–PVP–TiO_2 composite hollow fiber membranes for oily wastewater treatment using submerged membrane system, *Desalin. Water Treat.*, 2013, **51**, 1–11.

14 H. Ma, K. Yoon, L. Rong, Y. Mao, Z. Mo, D. Fang, Z. Hollander, J. Gaiteri, B. S. Hsiao and B. Chu, High-flux thin-film nanofibrous composite ultrafiltration membranes containing cellulose barrier layer, *J. Mater. Chem.*, 2010, **20**, 4692–4704.

15 B. Chakrabarty, A. K. Ghoshal and M. K. Purkait, Ultrafiltration of stable oil-in-water emulsion by polysulfone membrane, *J. Membr. Sci.*, 2008, **325**, 427–437.

16 J. Lee and T. Frankiewicz, Treatment of produced water with an ultrafiltration (UF) membrane – a field trial, in *SPE Annual Technical Conference and Exhibition*, 2005.

17 C. Wu, A. Li, L. Li, L. Zhang, H. Wang, X. Qi and Q. Zhang, Treatment of oily water by a poly(vinyl alcohol) ultrafiltration membrane, *Desalination*, 2008, **225**, 312–321.

18 Y.-R. Qiu, H. Zhong and Q.-X. Zhang, Treatment of stable oil/water emulsion by novel felt-metal supported PVA composite hydrophilic membrane using cross flow ultrafiltration, *Trans. Nonferrous Met. Soc. China*, 2009, **19**, 773–777.

19 I. Sadeghi, A. Aroujalian, A. Raisi, B. Dabir and M. Fathizadeh, Surface modification of polyethersulfone ultrafiltration membranes by corona air plasma for separation of oil/water emulsions, *J. Membr. Sci.*, 2013, **430**, 24–36.

20 D. M. Krstić, W. Höflinger, A. K. Koris and G. N. Vatai, Energy-saving potential of cross-flow ultrafiltration with inserted static mixer: Application to an oil-in-water emulsion, *Sep. Purif. Technol.*, 2007, **57**, 134–139.

21 C. Teodosiu, O. Pastravanu and M. Macoveanu, Neural network models for ultrafiltration and backwashing, *Water Res.*, 2000, **34**, 4371–4380.

22 Y. Zhu, F. Zhang, D. Wang, X. F. Pei, W. Zhang and J. Jin, A novel zwitterionic polyelectrolyte grafted PVDF membrane for thoroughly separating oil from water with ultrahigh efficiency, *J. Mater. Chem. A*, 2013, **1**, 5758–5765.

23 Y. Shang and Y. Peng, Research of a PVA composite ultrafiltration membrane used in oil-in-water, *Desalination*, 2007, **204**, 322–327.

24 L. Zou, I. Vidalis, D. Steele, A. Michelmore, S. P. Low and J. Q. J. C. Verberk, Surface hydrophilic modification of RO membranes by plasma polymerization for low organic fouling, *J. Membr. Sci.*, 2011, **369**, 420–428.

25 Y. Mansourpanah, S. S. Madaeni, A. Rahimpour, A. Farhadian and A. H. Taheri, Formation of appropriate sites on nanofiltration membrane surface for binding TiO_2

photo-catalyst: Performance, characterization and fouling-resistant capability, *J. Membr. Sci.*, 2009, **330**, 297–306.

26 M.-L. Luo, J.-Q. Zhao, W. Tang and C.-S. Pu, Hydrophilic modification of poly(ether sulfone) ultrafiltration membrane surface by self-assembly of TiO_2 nanoparticles, *Appl. Surf. Sci.*, 2005, **249**, 76–84.

27 J. Kim and B. Van der Bruggen, The use of nanoparticles in polymeric and ceramic membrane structures: Review of manufacturing procedures and performance improvement for water treatment, *Environ. Pollut.*, 2010, **158**, 2335–2349.

28 A. L. Ahmad, M. A. Majid and B. S. Ooi, Functionalized PSf/SiO_2 nanocomposite membrane for oil-in-water emulsion separation, *Desalination*, 2011, **268**, 266–269.

29 K. M. Parida, S. B. Kanungo and B. R. Sant, Studies on MnO_2—I. Chemical composition, microstructure and other characteristics of some synthetic MnO_2 of various crystalline modifications, *Electrochim. Acta*, 1981, **26**, 435–443.

30 Y. Liu, X. Yue, S. Zhang, J. Ren, L. Yang, Q. Wang and G. Wang, Synthesis of sulfonated polyphenylsulfone as candidates for antifouling ultrafiltration membrane, *Sep. Purif. Technol.*, 2012, **98**, 298–307.

31 J.-N. Shen, D.-D. Li, F.-Y. Jiang, J.-H. Qiu and C.-J. Gao, Purification and concentration of collagen by charged ultrafiltration membrane of hydrophilic polyacrylonitrile blend, *Sep. Purif. Technol.*, 2009, **66**, 257–262.

32 R. Jamshidi Gohari, W. J. Lau, T. Matsuura and A. F. Ismail, Fabrication and characterization of novel PES/Fe–Mn binary oxide UF mixed matrix membrane for adsorptive removal of As(III) from contaminated water solution, *Sep. Purif. Technol.*, 2013, **118**, 64–72.

33 M. Khayet, K. C. Khulbe and T. Matsuura, Characterization of membranes for membrane distillation by atomic force microscopy and estimation of their water vapor transfer coefficients in vacuum membrane distillation process, *J. Membr. Sci.*, 2004, **238**, 199–211.

34 T. Gumi, M. Valiente, K. C. Khulbe, C. Palet and T. Matsuura, Characterization of activated composite membranes by solute transport, contact angle measurement, AFM and ESR, *J. Membr. Sci.*, 2003, **212**, 123–134.

35 F. Pagnanelli, C. Sambenedetto, G. Furlani, F. Vegliò and L. Toro, Preparation and characterisation of chemical manganese dioxide: Effect of the operating conditions, *J. Power Sources*, 2007, **166**, 567–577.

36 E. Eren, B. Afsin and Y. Onal, Removal of lead ions by acid activated and manganese oxide-coated bentonite, *J. Hazard. Mater.*, 2009, **161**, 677–685.

37 C. Dong, G. He, H. Li, R. Zhao, Y. Han and Y. Deng, Antifouling enhancement of poly(vinylidene fluoride) microfiltration membrane by adding $Mg(OH)_2$ nanoparticles, *J. Membr. Sci.*, 2012, **387–388**, 40–47.

38 A. K. Nair, A. M. Isloor, R. Kumar and A. F. Ismail, Antifouling and performance enhancement of polysulfone ultrafiltration membranes using $CaCO_3$ nanoparticles, *Desalination*, 2013, **322**, 69–75.

39 J.-E. Zhou, Q. Chang, Y. Wang, J. Wang and G. Meng, Separation of stable oil–water emulsion by the hydrophilic

nano-sized ZrO_2 modified Al_2O_3 microfiltration membrane, *Sep. Purif. Technol.*, 2010, **75**, 243–248.

40 S. S. Madaeni and N. Ghaemi, Characterization of self-cleaning RO membranes coated with TiO_2 particles under UV irradiation, *J. Membr. Sci.*, 2007, **303**, 221–233.

41 F. L. Hua, Y. F. Tsang, Y. J. Wang, S. Y. Chan, H. Chua and S. N. Sin, Performance study of ceramic microfiltration membrane for oily wastewater treatment, *Chem. Eng. J.*, 2007, **128**, 169–175.

42 Y. Zhao, W. Xing, N. Xu and F.-S. Wong, Effects of inorganic salt on ceramic membrane microfiltration of titanium dioxide suspension, *J. Membr. Sci.*, 2005, **254**, 81–88.